Development of Aircraft Electric Starter-Generator System Based-On Active Rectification Technology

Serhiy Bozhko, *Member, IEEE*, Tao Yang, *Member, IEEE*, Jean-Marc Le Peuvedic,. Puvan Arumugam, Marco Degano, Antonino La Rocca, Zeyuan Xu, Mohamed Rashed, Weeramundage Fernando, Christopher Ian Hill, Carol Eastwick, Stephen Pickering, Chris Gerada, Patrick Wheeler, *Member, IEEE*

***Abstract*— More-electric aircraft (MEA) has become a dominant trend for modern aircraft. On-board MEA, many functions, which are conventionally driven by pneumatic and hydraulic power, are replaced with electrical subsystems. Starting aircraft engines with an electrical motor instead of using pneumatic power from the auxiliary power unit (APU) is one of the major characteristics of future aircraft. This paper presents the development of a novel electric starter-generator system for aircraft applications. The paper describes the main achievements of the project within the key areas including electric machines, power electronic converters, thermal management and overall system control design. The developed prototype has been tested successfully and the test results are presented in this paper.**

***Index Terms*— Active front-end, electric machine, more-electric aircraft, starter generator, thermal management**

I. Introduction

Due to the global efforts towards environmentally responsible air transportation, many aircraft systems technologies are currently undergoing significant changes. The state-of-the art technologies in the field are expected to be more fuel efficient, safer, simpler in servicing and of easier maintenance. The way towards this goal has been identified as a move towards "More-Electric Aircraft" (MEA) by replacement of hydraulic and pneumatic sources of power with electrical counterparts [1, 2]. The trend towards MEA relies on the facts that the electric power driven subsystems can achieve a higher efficiency compared to conventional pneumatic or hydraulic solutions. A high efficiency electrical solution will have the following advantages:

- A higher efficiency at the peak power allows a lower rated power installation in the upstream systems, which include power distribution, power generation, engine gearbox etc. The nacelle cooling and engine power extraction systems can all be made smaller and lighter, which translates into fuel savings.
- A higher overall efficiency will minimize the fuel consumption caused by on-board systems and reduce the overall fuel consumption of an aircraft, if the efficiency increase is achieved with low weight penalty.
- A higher efficiency benefits all the MEA technologies when compared to their conventional counterparts. It also eases requirements imposed on the engine, engine gearbox and nacelle cooling.

These potential benefits will lead to an increased reliance on electrical power for a range of primary functions including actuation [2], de-icing, cabin air-conditioning, and engine start. A large and global investment in MEA technologies will find practical and real applications only if low mass and high efficiency are achieved simultaneously. Improving the efficiency and reducing the mass of the electrical generation and distribution subsystems are two essential directions moving towards MEA.

The current starter/generators (S/G) typically employ a three-stage wound-field synchronous generator [2]. This machine has been extensively adopted in fixed wing and rotor craft applications and has proven to be highly reliable, and inherently safe, with voltage control achieved by varying the excitation current. Within aircraft the exciter is employed as a starter and exciter stator windings are designed for higher currents than required for power generation. Therefore the design cannot be regarded as optimal. The three-stage S/G has several constraints and disadvantages:

- These three-stage S/Gs cannot run over 20krpm due to its wound rotors embedded with rotating diodes. Running at high-speed may results in mechanical failure of the S/G. Indeed, most three-phase alternators rotate at 12krpm (15krpm max)
- The current S/G utilises a very different control scheme for the starting mode and the generation mode. This constrains the system design and leads to increased system complexity (addition of bleeders, etc…)

This work as supported in part by the EU PF7 Funding via the CleanSky JTI – system for green operations ITD through the AEGART project (No. 296090).

Serhiy Bozhko, Tao Yang, Puvan Arumugam, Marco Degano, Antonino La Rocca, Zeyuan Xu, Mohamed Rashed, Weeramundage Fernado, Christopher Hill, Carol Eastwick, Stephen Pickering, Chris Gerada and Patrick Wheeler are with the University of Nottingham (corresponding authors Serhiy.Bozhko@nottingham.ac.uk ; Tao.Yang@nottingham.ac.uk)

Jean-Marc Le Peuvedic is with Dassault Aviation (email: Jean-Marc.Le-Peuvedic@dassault-aviation.com)

- The state of the art 24 krpm 115V or 230V variable-frequency alternating-current (VFAC) S/G has a relatively high power density, but can only deliver a small fraction of the generation power in starting mode (most are found on APUs and the biggest ones are on B787 main engines)

Advances in power electronics result in the possibility to consider other machine types for the S/G operations which have the potential of a substantial improvement in power density (kW/kg), overall system performance, functionality, reliability, diagnostics, and availability for the overall system compared to the previous or existing solutions.

The AEGART project [3] (stands for Aircraft Electrical Starter-Generation System with Active Rectification Technology) targeted the development of such a novel system. The AEGART project aim was to develop an efficient and lower-mass S/G system for next-generation business Jet applications. The AEGART project aimed to deliver 20% lower mass and 10% better efficiency than comparable conventional starter/generators with better or improved safety. This project was part of "Eco-Design for Systems" ITD within CleanSky JTI and has become a cornerstone of the MEA. Some of the key features of the AEGART system have been described in TABLE I.

TABLE I Key features of AEGART system

Key features	Description
Operation speed range	0 - 32,000rpm
Continuous electrical power delivered	45kW with 270Vdc voltage source:
Maximum power can be delivered by the permanent magnet machine	can go up to 150kW with increased DC-link voltage
Cooling of the machine	Stator cooling
Cooling of the power converter	Power converter is located at the power electronics bay and thus liquid cooling is not available. Forced air cooling is used in the AEGART

Consideration of many design aspects was required for this complex multi-disciplinary task including definition of the best system topology, electrical machine and power electronic converter design, thermal management and cooling arrangements, development of control techniques, health monitoring and fault management systems. This paper reports the final achievements of the AEGART project. One of the challenges encountered in the design of a starter/generator for aero-engines is the need to satisfy the two fundamental functions, namely to provide mechanical power to the engines during start-up (as a starter) and to generate electrical power during normal engine operation (as a generator). The developed solution utilizes recent advances in modern power electronics allowing the use of novel machine types together with the introduction of controlled power electronic converters into the main path of energy flow. This paper summarized the AEGART project including machine design, power converter design and S/G testing. Different aspects of the project have been reviewed and the main results achieved have also been presented in this paper.

II. BASIC CONCEPT

This section gives a brief introduction of the concept of a starter/generator system. The starter/generator system is essentially a system which allows bi-direction power flow between two voltage sources.

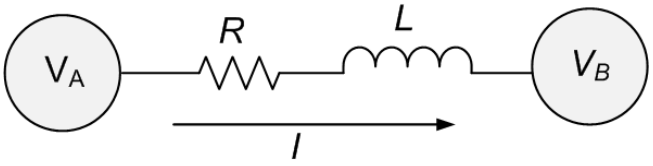

Figure 1 Example circuit

Consider a simple RL-electric circuit connected to two voltage sources V_A and V_B on each side, as shown in Figure 1. If we assume that voltage source V_A is fixed. Varying the magnitude and the phase of the source V_B, the current in the circuit can be controlled in both the magnitude and the phase with respect to V_A. It means that the power flow through the circuit (active P and reactive Q) can be controlled in either direction. If the role of V_A is given to the electric machine, and the role of V_B – to the power electronic converter that acts as a voltage source, then one can control the machine as a motor (directing the active power flow to machine) or as a generator (power is extracting from the machine) as illustrated by Figure 2.

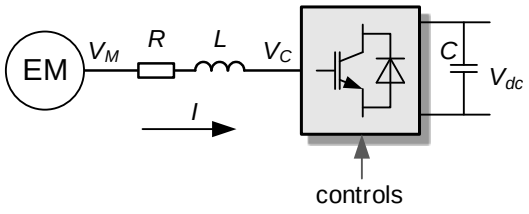

Figure 2 Electric Machine – Power Converter system

The developed AEGART S/G system implements the described idea. The speed-torque characteristic requirement of the S/G is shown in Figure 3. The machine runs as a motor during the engine starting period. During this period, the power is flowing from the converter to the electric machine. When the engine is self-sustained, it starts to drive the electric machine as a generator and the power starts to flow from the electric machine to the converter. The dc-link voltage of the power converter is set at 270VDC. An approximate torque speed characteristics requirement of the starter generator is shown in Figure 3. As can be seen, the machine runs as a motor during engine start to ω_{start}. The engine ignites at the speed ω_{start} and starts to drive the machine to the speed ω_{min}, where the machine will start to run as a generator. The speed range for the electric machine running as a generator is from ω_{min} (20,000rpm) to ω_{max} (32,000rpm). When running as a generator, the electric machine can supply a maximum constant power of 45 kW.

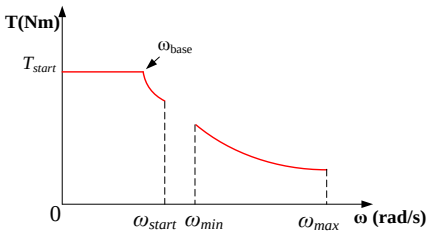

Figure 3 Torque-Speed characteristics of the aircraft starter-generator

Different electrical machine topologies, namely induction machines, switched reluctance machine [4, 5] and topological variants of permanent magnet based machines [6, 7] were considered together with their respective driving converters during the trade-off study period with the process shown in Figure 4.

Initially, the identified machine types have been subject to a basic design analysis to establish the optimal aspect ratio, cross section, to guarantee a mechanical integrity, to define a number of turns to suit the required DC-side voltage, etc. Based on these criteria, the possibility of achieving a peak torque has been assessed. If failed, then the next approximation cycle was initiated with modified initial selections. If the peak torque can be achieved, then the next stage of design was undertaken: this includes calculation of machine losses and calculation of machine lumped parameters. In parallel, each machine type requires an appropriate converter topology and thermal arrangement. These were included into the trade-off process as well, as Figure 4 shows. A machine lumped parameter model, together with the converter topology candidate, allows for calculation of converter losses and design of basic heatsink. Machine losses, together with possible machine cooling arrangements, allows for assessment of machine temperature – if this appears to be higher than allowed, then another cycle of basic design is required. If passed, then the total system mass and system efficiency can be evaluated, as well as system reliability and safety.

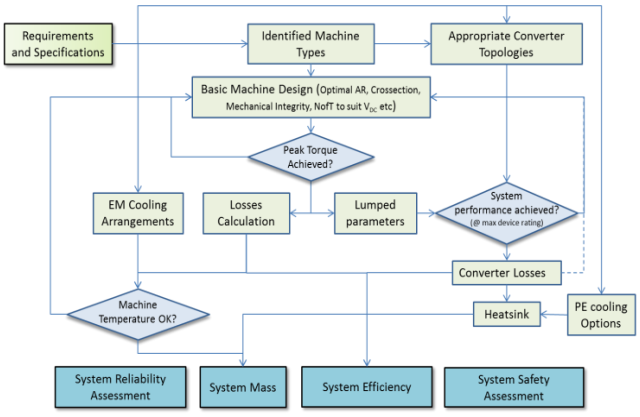

Figure 4 Illustration of AEGART trade-off process

As the trade-off study result, for the detailed development of the AEGART system, the topology "permanent-magnet machine with surface-mounted magnets (SPM) with three-level IGBT converter" was selected.

III. Electric Machine Design

In the design process, fault tolerance is considered by adopting a redundancy solution in the event of a failure. This allows a distributed winding to be adopted, consequently minimizing rotor losses in both permanent magnet and the rotor back iron. Different slot-pole combinations were investigated in view of the overall losses and performance and the compromise in the design of the machine for operating as an engine starter and as generator. Implications of different magnet's retention material and magnetic materials were studied.

A. Slot/pole combinations

The slot (Q) /pole (p) combinations considered during design are shown in Table I. Both single (N_{lay} = 1) and double layer (N_{lay} = 2) winding topologies are considered in the selection procedure. The number of rotor poles is limited to 4, 6 and 8 as any higher number of poles will lead to high electrical frequencies and higher power converter losses. In order to limit the temperature increase in the rotor as a consequence of the eddy currents induced by magnetomotive force (MMF) harmonics at high speed, the winding topology for each slot/pole combination was considered such that the winding harmonics are minimized for an acceptable trade-off with the fundamental winding factor.

TABLE II Considered slot/pole combinations

Q	N_{lay}	2p	Q	2p	Q	2p	Q
0.5	2	4	6	6	9	8	12
1	1	4	12	6	18	8	24
1	2	4	12	6	18	8	24
1.5	2	4	18	6	27	8	36
2	1	4	24	6	36	8	48
2	2	4	24	**6**	**36**	8	48

Normally, the highest efficiency can be achieved by machines with higher pole numbers. However, a high pole number will result in a higher fundamental frequency of the machine and thus require a higher switching frequency of the power converter. With these considerations, the 6-pole machine designs were considered for the final machine design. Out of the 6-pole machine variants, the best machine candidate was selected as 6-poles 36-slots as it has the lowest eddy-current losses.

Table III represents the winding factors associated with different slot-per-pole-per-phase (q) and winding layer number combinations considered in the comparison designs, where the parameter r_c represents the coil pitch.

TABLE III Winding factors associated with different slot-per-pole-per-phase and winding layer number combinations

			Winding factors of prominent harmonics					
q	N_{lay}	r_c	*1*	*2*	*4*	*5*	*7*	*11*
0.5	2	1	0.866	0.866	0.866	0.866	0.866	*
1	1	3	1	0	0	1	1	1
1	2	2	0.866	0	0	0.866	0.866	0.866
1.5	2	4	0.945	0.061	0.140	0.140	0.061	*
2	1	5	0.966	0	0	0.259	0.259	0.966
2	2	5	0.933	0	0	0.067	0.067	0.933

** represent cases where non-zero intermediate values exist between the 7th and the 11th harmonic orders.*

When comparing the different slot/pole combinations, in each design, the stator tooth maximum flux density at no-load was considered to have 75% of the saturation flux density of the core material. The total weight of each machine was maintained the same for the comparative study. This included the stator, rotor and the copper associated with the winding, including the end windings. Each machine was thus designed for a constant weight and fixed outer diameter so as to fulfil the torque-speed criteria presented in Figure 3. The final selection of the winding configurations is made to be slot-per-pole-per-phase q=2, winding layer number to be 1 and coli pitch r_c to be 5 due to its lower harmonics.

B. Implication of Magnet retention

To retain the surface magnet, two different sleeve materials were investigated during the design period: Carbon Fiber (CF) and Inconel 718. The sleeve thickness calculation was performed based on a 110% over-speed safety margin (i.e. designed at 32,000rpm *110% =35,200rpm) . The relation between the sleeve thickness and the rotor radius with different magnet thickness is shown in Figure 5.

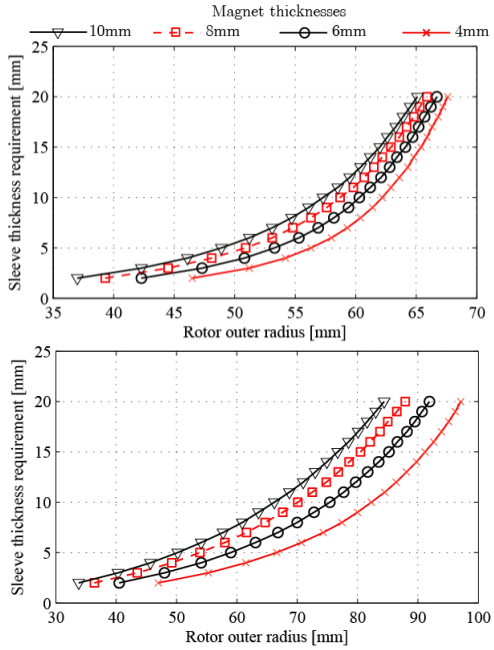

Figure 5 Variation of sleeve thickness requirement with rotor outer diameter: above, Carbon fibre sleeves; below, Inconel sleeves

It can be seen that the required sleeve thickness is highly influenced by the rotor radius. This is due to the fact that the centrifugal force proportionally increases with the rotor radius. The magnet thickness, however, has a less significant influence over the sleeve thickness requirement. It was identified that the carbon fibre sleeve was required to be thicker than that of the Inconel sleeve, especially when the rotor radius is beyond 60mm.

The pre-stress of the 4 mm sleeve of CF and Inconel at maximum speed (32krpm) is shown in Table III. Both sleeves provide reasonable pre-stress with corresponding sleeves. The CF has been the final choice since it has negligible eddy current losses compared to Inconel sleeve. The eddy losses of the electrical machine is estimated using Finite Element Software MAGNET. The maximum Eddy losses were achieved at 32,000rpm at rated power 45kW. The stress plot of the rotor with the CF sleeve at 32,000rpm with the worst temperature is shown in Figure 6. It can be seen that the maximum stress under the worst case scenario (highest operational speed 32,000rpm), is around 715 MPa which is within safe margin of the given CF sleeve's allowable stress.

TABLE IV. Mechanical parameters of Carbon Fiber and Inconel sleeves at the maximum speed 32krpm

Parameter	*Carbon Fiber*	*Inconel Alloy*
Sleeve thickness (mm)	4	4
Sleeve undersize (mm)	0.134	0.308
Sleeve prestress (MPa)	510	676
Eddy losses at 32,000rpm (W)	12.1	383.7

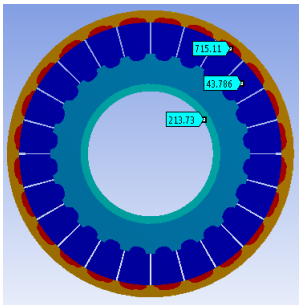

Figure 6 Stress plot of machine rotor with the Carbon Fiber sleeve at 32 krpm and under a worst case temperature gradient of 200^{0}C sleeve, 170^{0}C magnets and 120^{0}C rotor core

C. Magnetic material selection

From Figure 3, it is possible to identify that the designed machine will be working under flux weakening conditions with a wide speed range (speed from ω_{base} = 12,000rpm up to 32,000rpm). Under the flux weakening conditions, the machine magnet will be handling demagnetizing current injected from the machine terminals. In order to prevent a design of a machine with a high demagnetization risk, the maximum demagnetization field condition is incorporated in the design process The magnets are arranged in a Halbach structure using Samarium cobalt magnet (Sm_2Co_{17}) material. Magnet demagnetization at different operating points is considered and the designs are modified when it was subject to strong demagnetization field.

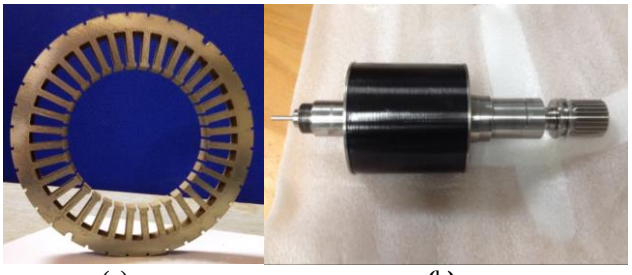

(a) **(b)**

Figure 7. AEGART machine: manufactured stator and rotor. (a) cross-section view of the manufactured 36 slot stator; (b) manufactured rotor with CF sleeves

D. Magnet Demagnetization

Operating conditions in both motoring and generating modes demand high currents which may result in high demagnetization fields. In order to prevent a design of a machine with a high demagnetization risk, a maximum demagnetization field condition is incorporated in the design process. Based on the cooling available, worst-case rotor temperature for the aero-engine starter-generator is considered at 300°C. The magnets are arranged in Halbach structure using Samarium cobalt magnet (Sm_2Co_{17}) material. Magnet demagnetization at different operating points is considered and the designs are modified when it was subject to strong demagnetization field.

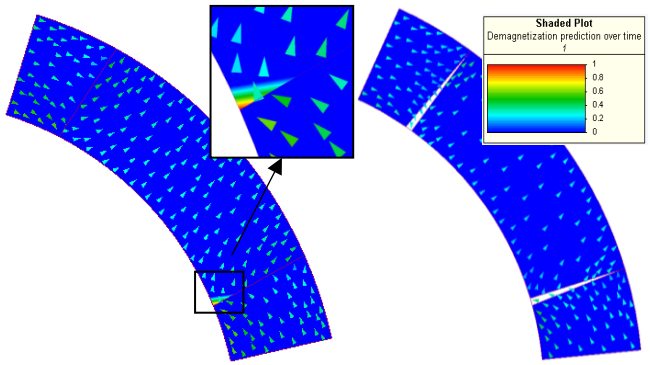

(a) (b)

Figure 8 Demagnetization prediction plot at maximum speed

Figure 8a shows the demagnetization prediction plot obtained in FE at 32 krpm under worst case temperature. The constant value of 1 shown in the plot represents the magnet under risk of demagnetization whilst 0 is no demagnetization risk. From the results, it can be clearly seen that there are slight demagnetization effects during generating mode. This is due to the magnet arrangement of the Halbach structure. To avoid the demagnetization on the edges, the magnets are modified as shown in Figure 8b. From Figure 8b, it can be clearly seen that the magnets are not subject to demagnetization.

E. Thermal management

The thermal design of the developed starter/generator has been detailed in [8] and will be only briefly discussed in this paper. During the design process, the following aspects were accounted for in design of an optimised cooling system:

- *Effectiveness*: Intensive cooling can improve the overall machine efficiency by reducing the temperature dependent losses such as copper losses.
- *Reliability:* High temperatures accelerate the aging of some components, reducing their lifetime; hence operating at low temperatures can increase the overall reliability of the machine. As an example, a temperature rise of 10°C can reduce the winding insulation life by around 50% [9].
- *Reduction of size and weight*: In aerospace applications, size and weight are particularly significant factors to be taken into account, having a direct impact on the fuel consumption and hence CO_2 emissions.

Direct oil cooling of the machine stator was identified as the optimal solution. The core principle utilised for machine cooling was to use ducts through the stator core along the stator outer diameter and the slots existing between stator teeth. This arrangement guaranteed an even distribution of the coolant. An electrically non-conductive sleeve separated the airgap and rotor from the stator. This solution keeps windage losses manageable (windage loss is the viscous friction loss generated between a fluid and the rotating elements). The electromagnetic losses (including copper loss, eddy current losses in magnets and iron losses) were derived using co-simulation of FE machine model and power converter in Matlab/Simulink. The windage loss was estimated both numerically (CFD) and analytically whilst bearing losses where only analytically predicted as detailed in [10]. Further enhancing cooling techniques, such as radial jets at the drive end and a flow deflector at the non-drive end were also implemented to improve system efficiency and hence reduce machine weight.

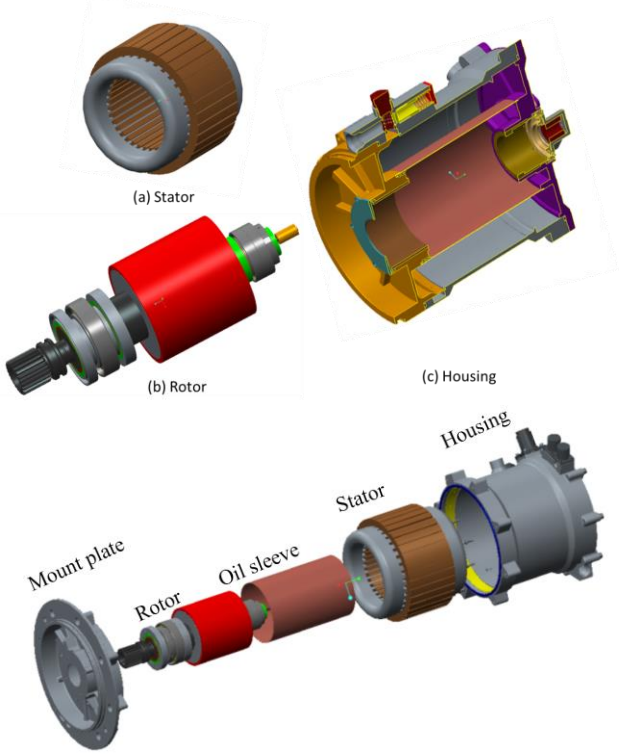

Figure 9 Main components of the designed starter/generator

F. Mechanical design

The detailed mechanical design of the machine is presented in our previous publications [8]. The final rotor, stator and machine housing are shown in Figure 9. The rotor shaft is made of high strength stainless still with a diameter of 40mm and a length of 250mm. The shaft is connected to a gear box through a spline at the drive end. At the non-drive end, a resolver is connected for speed measurement and control applications. The shaft is supported by bearings at each end mounted in the two flanges of the machine. The stator, made of iron laminates and copper windings, was directly inserted into the machine casing. The rotor consisted of a shaft and magnets, and was inserted into the stator central chamber,

supported at both ends by bearing sets fitted within the machine casing.

IV. Power Electronic Converter

From the machine preliminary design, the boundaries for the converter were defined as 400A peak output current, 1.2kV DC-link peak and an electrical frequency equal to 1.6 kHz, given the three pole pairs of the machine. During the design process, both conventional two-level converters and three-level neutral point clamped (NPC) converters [11, 12] were considered.

A two-level converter was considered for its known simplicity and intrinsic reliability due to the minimal number of devices. A three-level converter was also considered because it brings advantages of lower EMI emissions [13], better power quality and ablility to handle higher fundamental compared with two-level converters. This is a useful feature when considering the high speed application of this drive. In addition, the voltage across the switches is only half the dc bus voltage. This feature effectively doubles the power rating of the converter for a given power semiconductor device. When used as an inverter, the first group of voltage harmonics on the AC side is centred around twice the switching frequency. This feature enables further reduction in size and cost of passive components while at the same time improving the quality of the output waveform.

The final decision, however, came from the power loss comparison for these two topologies. Since more power losses would mean increase of cooling system capacity and thus more weight and volume of the whole power converter system. In order to estimate the power losses of power converters, simulation studies were performed using Matlab PLECS toolbox with the thermal characteristics of actual semiconductor devices imported and implemented in the simulation modules. The total losses of the converter were simulated and calculated for different operational conditions.

The power converter losses of two-level and three-level converters are compared using Infineon modules (two-level with modules FF450R12IE4 modules, three-level with F3L400R07ME4 modules). The two-level converter is implemented using 450A/1.2kV modules, and the modules for three-level converter are rated at 400A/650V (the voltage requirement for power modules of three-level converter is half of that required for the two-level converter due to the fact that there are two power modules in series at each half leg of the three-level topology). Figure 10 shows the comparison of losses for these two converters, operating at different speed conditions with full power (speeds at ω_{start}, ω_{min} and ω_{max}). The switching frequency is set at 16kHz.

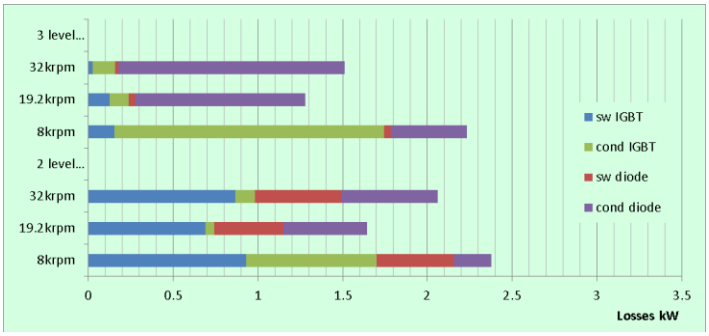

Figure 10 Losses comparison for two-level and three-level converters when the S/G operates at different conditions (running as a starter @8krpm; running as a generator @ 19.2krpm and 32krpm)

From Figure 10, it can be seen that the total power losses in a converter consist of the switching and conduction losses of the IGBTs (sw IGBT, cond IGBT) and the diodes (sw diode, cond diode). Through simulations using Matlab/PLECS toolbox, these four types of power losses can be conveniently derived. The three-level converter has much less power losses under different operating conditions, as it is seen from Figure 10. The power loss distribution under different operating conditions is also different between two-level and three-level converters. During the motoring mode (ω=8,000rpm), for the two-level converter, the conduction and switching losses of the IGBTs contribute most of the power losses. For the three-level converters, however, most of the power losses are from IGBT conduction losses. This is due to the fact that the three-level converter has lower voltages across its IGBTs during the switching-on process. During generation mode, the power losses within three-level converters are predominantly contributed from the diode conduction losses. This is due to the fact that the current will flow mostly through the diodes during generation mode. Considering the fact that the three-level NPC converter has less power losses and higher power quality, this converter topology was selected for detailed design and manufacturing.

The thermal management system for the converter was designed based on the estimated power losses under the worst-case scenario, namely when the unsuccessful start is followed by another starting attempt after 3 minutes interval. A forced air-cooled solution was employed and the heatsink for the power modules was designed to guarantee an acceptable temperature at the end of the worst-case scenario. The prototype for the designed power converter is shown in Figure 16 in section VII.

V. Control Design

The detailed design process for the starter/generator system has been reported in previous publication [14-17]. A cascaded control scheme was used for the starter/generator system control as shown in Figure 11.

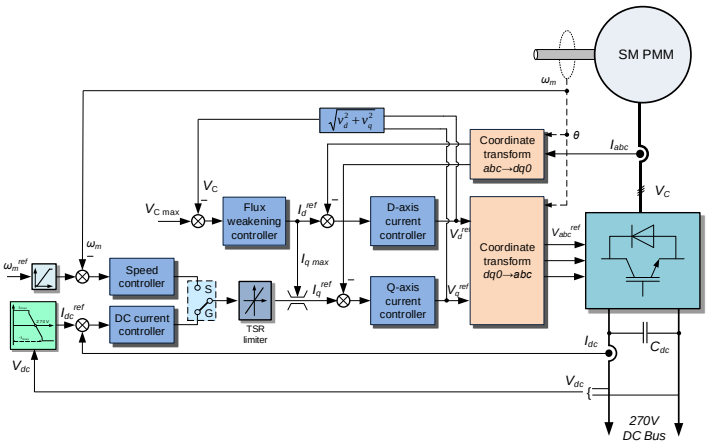

Figure 11. Control diagram for developed starter/generator system

The internal loop is for current control. The external loop includes flux weakening control, speed control (when running as a starter) and dc-link current control (when running as a generator). The vector control scheme was used to for the machine current loop control. This control technique has been widely used for electric machine control [18]. Within the vector control scheme, the stator current vector is represented in a rotating reference frame (*dq* frame) with its d axis aligned with the rotor flux. By doing this, the d-axis and q-axis components of the PMSM stator currents can be controlled independently. The machine torque, or active power, is controlled by the q axis current. Flux-weakening control can thus be achieved by injecting negative currents into the d axis. As can be seen in Figure 11, the flux weakening controller takes the error between the maximum AC voltage which can be provided by the converter, $V_{c,max}$ (i.e. $V_{dc}/\sqrt{3}$) and Vc (magnitude of the voltage vector at converter AC terminals and it is calculated from the output of the current loop controller) and generates the flux weakening current reference I_d^{ref}. Since the AC voltages at the converter are modulated containing switching harmonics, we take the voltage references V_d^{ref} and V_q^{ref} instead. The speed controller is activated when the electric machine is running as a starter. When the electric machine is running as a generator, the dc-link current i_{dc} is controlled according to the following droop characteristic (specified by the customer as shown in Figure 12 (a)):

$$i_{dc} = k_{droop}(270 - V_{dc}) \quad (1)$$

From the measured dc-link voltage, V_{dc}, the i_{dc} reference is derived according to (1) and the DC current is controlled to this value by a PI controller. With the droop control, the S/G system during the generation mode can essentially be viewed as an ideal dc source with a resistor connected in series as shown in Figure 12.

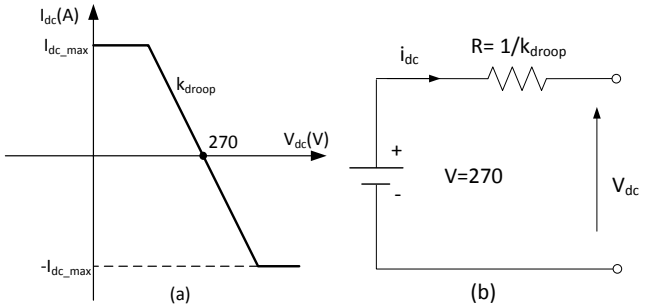

Figure 12 Representation of droop control for S/G systems during the generation mode. a) in diagram, b)An equivalent circuit

In the motoring mode (during the engine starting cycle), the electric machine is running as a motor under closed-loop speed control and driving the engine up to the speed at which the engine can be ignited. When the engine speed reaches the self-sustained speed, the controller will give a "ready-to-generate" signal and as the speed reaches the lowest generation value, the system reconfigures to run as a generator with generation droop control scheme as discussed above.

VI. Thermal Modelling and Design

A. Thermal modelling

The thermal modelling of the machine was carried out using both analytical (lumped parameter thermal network) and numerical (computational fluid-dynamics) approaches. Using FEM electromagnetics simulation (MAGNET), the power losses at the worst condition have been calculated and is shown in TABLE V.

TABLE V machine main power losses

Part	**Loss(W)**
Copper loss (at 180°C)	1,065
Stator Core	60
Magnets	50
Rotor core	9

The analytical models were particularly used in the preliminary design stage to investigate the thermal behaviour of initial electric machine and the performance of the existing cooling strategies. The commercial package employed for the analytical design, to produce the machine thermal network, is available on the market. In this particular project, we used MotorCAD.

However, the lumped parameter method is not fully capable of predicting all aspects of the fluid flow and the convective heat transfer phenomena. For this reason, some critical areas of the machine, such as the end regions, the axial ducts and the airgap were investigated using CFD. Some numerical data such as the convective heat transfer coefficients were then exported to MotorCAD in order to improve the accuracy of the thermal network.

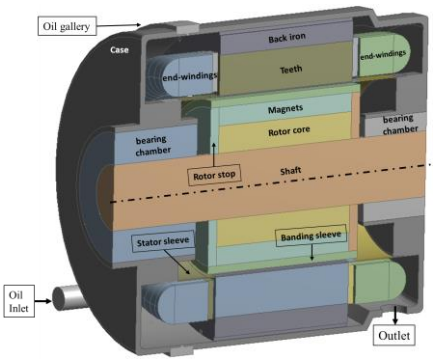

Figure 13. Cross-section of 3D Machine domain

A full 360° domain of the machine was modelled to perform steady-state conjugate heat transfer analysis. Due to the complexity of the real design several simplifications were made. These mainly consisted of the removal of small features such as screws, bolts and threads. Components such as coils, laminations and bearing chambers were modelled as bulk solids but overall thermal properties were assigned to these zones. Figure 13 shows a cross-section of the domain created.

Some areas, such as end regions and the air-gap, were separately investigated in order to have a better understanding of the fluid flow and to identify the optimal mesh densities to be used in the full model. Although the k-epsilon turbulence model is the most common model used in Computational Fluid Dynamics to simulate mean flow characteristics for turbulent flow conditions, the Realizable k-epsilon, which is a Reynolds-Averaged Navier-Stokes (RANS) based model, was the turbulence model used in the AEGART project. The Realizable k-epsilon model is a sub-model of the k-epsilon model and it is normally more appropriate for cases involving rotation, higher shear stresses, and higher pressure/velocity gradients [10]. This is because the Realizable k-epsilon can generally provide better performance than the classic Standard k-epsilon for cases involving rotation and high shear stresses. The rotation is modelled using the Multiple Reference Frame (MRF) technique. This technique is the most common technique used when simulating rotating domains; indeed this allow implementing the rotation without actually having a rotating mesh. This characteristic makes the MRF more suitable for steady-state cases and is less computationally demanding than the Sliding Mesh technique. Enhanced wall treatment was used to resolve complex near wall phenomena which may occur; this implies an accurate sizing of the first layer of inflation in order to get the required y+ ~ 1. The y+, also defined as dimensionless wall distance, is a parameter which determine the level of accuracy achievable in capturing near wall phenomena (interaction fluid/solid). The y^+ value used in Finite Element Analysis is a non-dimensional distance from the wall (boundaries) to the first mesh node; this is defined as $y^+ = \frac{y\, u_\tau}{\nu}$, where y, u_τ and ν are the wall distance, the shear velocity and the kinematic viscosity of the fluid respectively [17].

B. Thermal design

During the preliminary design process, a liquid cooling solution was identified considering the fact that liquid cooling techniques generally lead to more compact designs than air cooled machines as the aircraft engine lubrication oil is available [19]. An oil cooling solution was therefore selected for the electric machine within the starter/generator system.

Since the S/G electric machine is a high-speed application, a direct oil cooling (wet-rotor solution) method was not the optimal solution due the high windage loss (the viscous friction loss generated between a fluid and the rotating elements). Windage loss is directly proportional to the fluid viscosity and to the cube of the rotational speed (ω^3). Therefore significant viscous heat will be generated in the air-gap due the high-speed rotating machine. For a high-speed machine like S/G within AEGART, liquid must be avoided in the air-gap at all times.

Based on the above considerations, a wet stator solution was implemented for the developed starter/generator electric machine. This design guarantees intensive direct cooling of the stator. A stator sleeve was used to prevent liquid from entering the air gap. The concept is shown in Figure 14. Once the coolant enters the stator chamber, through several radial openings impinging over the end-windings, it flows through the stator core in two rows of axial ducts created through the stator laminations, one along the stator inner diameter and the other along the stator outer diameter, as shown in Figure 15 (concept only).

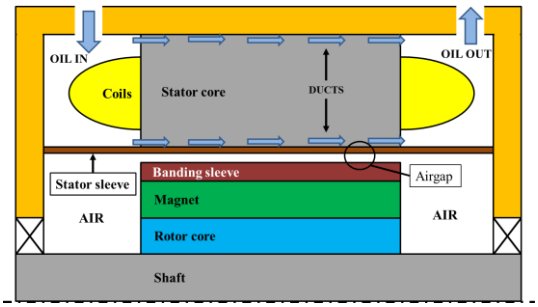

Figure 14. Schematic Wet Stator of the starter/generator electric machine [8]

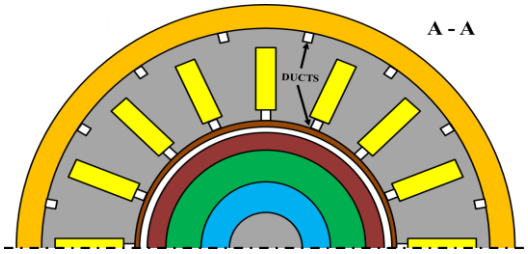

Figure 15. Layout of axial ducts within the electric machine [8]

VII. MANUFACTURING AND TESTING

After detailed design, the starter/generator system was manufactured and tested. The 6-pole, 36-slot machine design (B12) is prototyped to demonstrate its ability to produce the required torque-speed curve shown in Fig.1 and validate the design. Silicon steel is used for the stator. The stator windings include 2 turns per coil and 69 sub-strands for each turn. The rotor back-iron and the shaft consist of single body using semi-magnetic stainless steel PH 17-4. The Samarium cobalt

PMs (Sm_2Co_{17}) are arranged in Halbach array structure which is retained by directly wound CF sleeves. The prototyped stator, rotor and complete assembly of the starter-generator machine are shown in Figure 16. It is worth highlighting here that the mass density of the machine is 33*kW/L & 16kW/kg*.

The final system scheme for S/G functional test is also shown in Figure 16. During our test campaign, the S/G was coupled mechanically with a dynamometer machine which can be operated in four quadrants in the torque-speed plane.

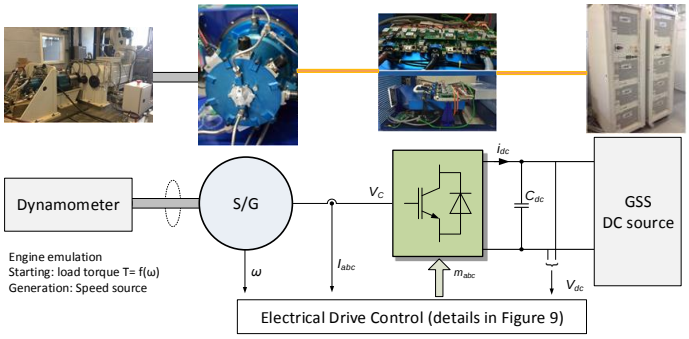

Figure 16. Testing bench for the S/G system, left to right: dynamometer, Starter/generator, power electronics and GSS DC source

The dynamometer allows operation in two modes: the torque control mode and the speed control mode. These two modes are used for testing the motoring and generation functions respectively. All these tests were conducted using facilities within the University of Nottingham and implemented at ambient temperature. The machine is pre-heated up to 50°C before test (this is due to the fact that 50°C is the minimum temperature at which the temperature management system functions properly)

A. Motoring mode test of S/G

During the S/G motoring mode test, the dynamometer behaves as a mechanical load to the S/G and represents the engine friction torque during engine start-up. When running as a mechanical load, the dynamometer is working in a torque control mode and the torque is controlled by its own controller. Since the engine friction torque is dependent on the engine shaft speed and the ambient temperature, different T-ω curves at different temperatures are expected. As can be seen from Figure 17, the reference torque T^* of dynamometer is dependent on the shaft rotational speed ω with the T-ω profiles pre-programmed in its controller before testing.

For aircraft applications, it is required that the S/G should be able to start up the engine successfully in any potential ambient temperature conditions. Two extreme cases were tested during the S/G system functional test campaign, i.e. ambient temperature T= 55°C (engine hot start-up condition) and T= -40°C (engine cold start-up condition). The T-ω curves used at these temperatures are provided by our industrial partner. Under these two conditions, the engine friction T and speed ω profile is shown in Figure 18.

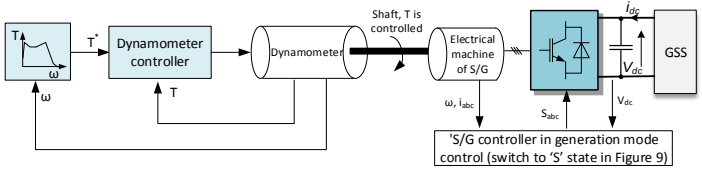

Figure 17. Dynamometer control when S/G is in the motoring mode

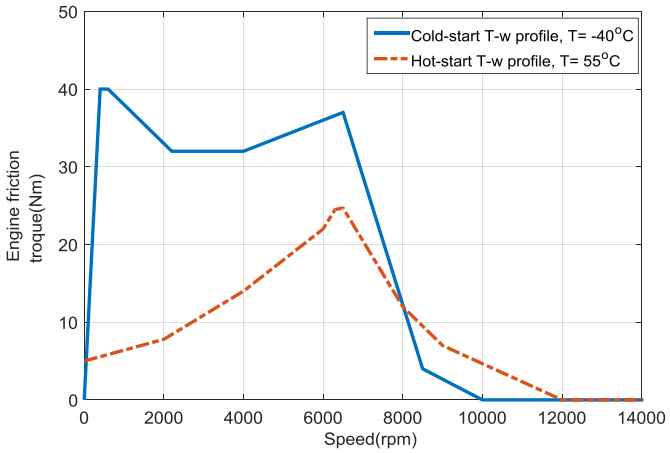

Figure 18 Engine friction torque corresponding to the engine speed during the starting process. Solid line: cold-start condition, dashed line: hot-start condition.

During the motoring mode test, it is required that the S/G should be able to accelerate aircraft engines up to 10,000rpm smoothly. The motoring test result under a cold-start torque profile is shown in Figure 19 (a1- d1). From the speed profile in Figure 19(a1), it can be seen that the S/G is able to smoothly accelerate the aircraft engine during a cold environment (-40°C) to a requested speed 10,000rpm in 40 seconds. Since the speed is lower than ω_{base}, there is no need for flux weakening operation, i.e. the current i_d = 0A. The electromagnetic torque T_e is proportionate to the q-axis current i_q and thus the current i_q reflects the cold-start torque profile as shown in Figure 19(b1). The temperatures of machine windings and the power converter are shown in Figure 19 (c1) and Figure 19 (d1). It can be seen that the maximum temperature is 60°C for the power converter devices and is 72°C for electric machine stator windings. Both temperatures are below the maximum allowed values. The temperature of power converter devices and electric machine windings are closely related to the active power (providing torque during motoring) current i_q. It can be seen that both machine and power converters reached their highest temperature simultaneously after i_q decreased from the maximum point (Figure 19 b1-c1).

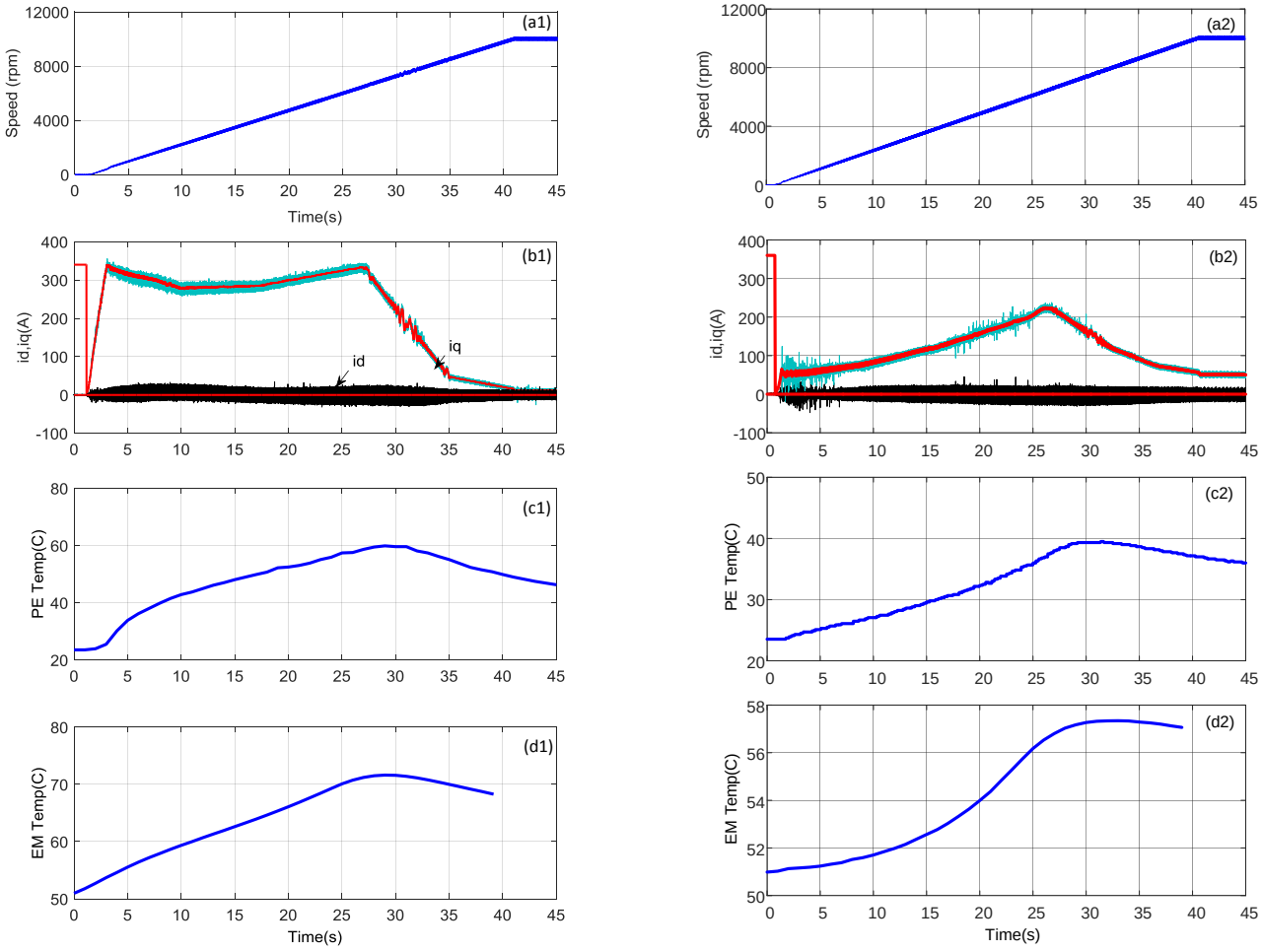

Figure 19 Machine speed, i_d. and i_q response starter/generator system for cold-start (a1- d1) and hot-start (a2- d2) conditions. a) speed response; b) id & iq; (a) Temperature of power converter, (b) Temperature response of electric machine stator windings

The hot-start testing results are shown in Figure 19 (a2 – d2). It can be seen that the machine successfully drove the engine up to 10,000rpm in 40 seconds time very smoothly. The current i_q of machine stator reflected the hot-start engine torque profile. Since the speed has not reached the flux-weakening range, the flux-control current i_d also kept at zero. The maximum temperature of the power converter during hot-engine start mode is about 40^{o}C and the maximum temperature of the electric machine is 57^{o}C. During the cold-start test, the maximum temperature is 60 ^{o}C for the power converter and 72 ^{o}C for the machine. Since both tests are with initial temperature conditions, the power converter and electrical machine during hot-start test are with much lower temperature rise. This is mainly due to the fact that under cold-start conditions, the engine friction torque is larger and more challenging thus requires more current i_q to produce electromagnetic torque and crank the engine.

B. Generation mode test of S/G

When the S/G system goes into generation mode, the S/G will be running as a generator driven by the engine. Under this condition, the dynamometer is used as the prime mover to drive the S/G. The dynamometer shaft speed is controlled to a reference value by its own controller. As illustrated in Figure 20, the dynamometer essentially behaves as a mechanical speed source during this mode and drives the S/G to any requested speed up to 32,000rpm (the maximum generation speed). The S/G transforms the mechanical power to electrical power and supplies electrical power to the loads (i.e. GSS as it is able to operate in four quadrant and thus can be used as a load).

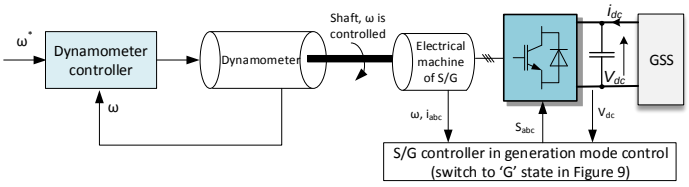

Figure 20 Dynamometer control when S/G is in the generation mode

As mentioned in Section V, during the generation mode test, a V-I droop characteristic is applied (in this test, the droop gain is set at K_{droop}=8.0). The load current i_{dc} is controlled to follow the droop characteristic dependent on the dc-link voltage v_{dc}. Within this test, the dc-link voltage v_{dc} is controlled by the GSS. With different v_{dc} set by the GSS, the S/G system will

supply a corresponding current i_{dc} according the droop characteristic. The derived v_{dc}-i_{dc} curve from generation mode test campaign is shown in Figure 21. It can be seen that the current i_{dc} supplied by the S/G system is well controlled and follows the pre-defined droop characteristic. In addition, when the v_{dc} is lower than 270V, the current i_{dc} is positive and the power is flowing from the generator to the GSS (the load). When v_{dc} is higher than 270V, the i_{dc} is negative and the power flows from the GSS to the generator (power regeneration).

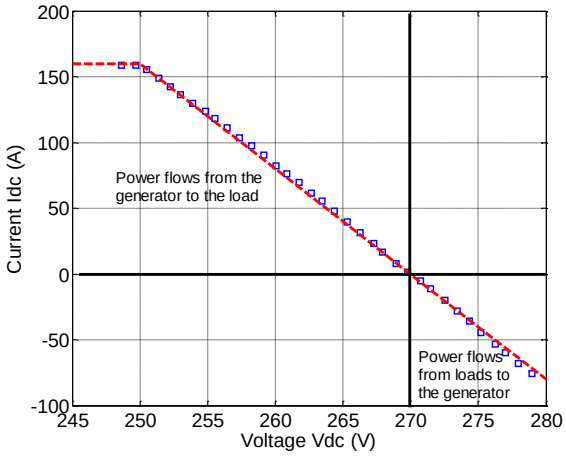

Figure 21 Droop characteristic test of S/G during generation mode

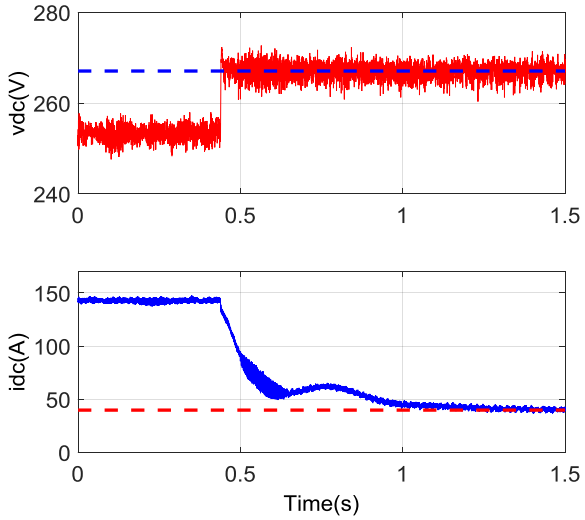

Figure 22 Transient response of step change of v_{dc}

The transient response on dc-link voltage v_{dc} step change (from 252V to 265V) is shown in Figure 22. The i_{dc} is changing according to the droop characteristic, from 140.5A to 39.2A. It can also be noticed that the transient of the i_{dc} is much slower than that of the v_{dc}. With a step change of v_{dc}, it is expected that i_{dc} should be a step change or with very fast transient due to the droop control. However, this may lead to a current surge in the electrical machines due to its fast current control loop (500Hz). To avoid this issue, a low-pass v_{dc} filter is added in the control loop (in DSP code). The machine thermal performance (and the machine thermal model) was investigated by carrying out Short Circuit Tests (SC Tests) up to 12,000 rpm. The SC test set-up is shown Figure 23.

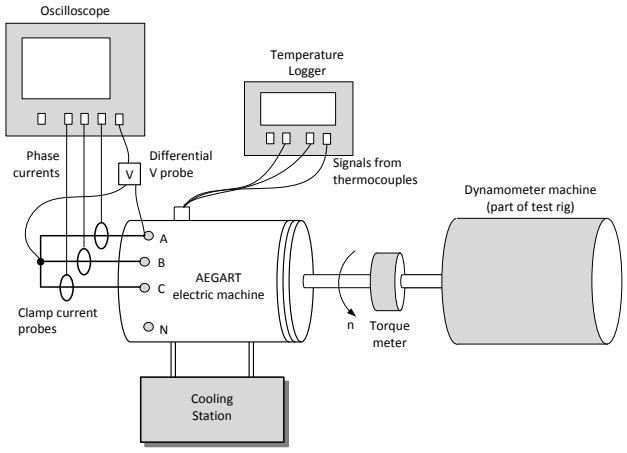

Figure 23. Short-circuit test set up for the AEGART project

The short-circuit test is following the steps below

1) Set the Oil Cooling station temperature to 50°C.
2) Connect the winding-located thermocouples to the temperature logger
3) Connect the phase terminals to a single bus-bar for terminal short-circuits tests.
4) Connect the current measurement units and voltage probe to an oscilloscope.
5) Start up the dynamometer machine and set the speed to 400rpm. Wait for thermal stabilization of the machine.
6) Measure the machine current, voltage and torque and capture the current waveforms.
7) Repeat steps 6-7 for speeds 800rpm, 1200rpm, 1600rpm, 2000rpm, 2500rpm, 3000rpm, 3500rpm and 4000rpm. Record the winding temperature at each step. Make sure the winding temperature does not exceed 180°C.
8) Increase the speed to 5000rpm. Observe that the machine current increases much less compared to the previous steps. Take measurements as in step 6.
9) Repeat step 8 for speed 8,000rpm.
10) Continue increasing speed by steps of 4,000rpm (until reached 12,000rpm) and take measurements as in step 6 after thermal stabilization of the machine.
11) Turn off the test bench.

In order to evaluate the performance of the final design some temperature measurements were taken; some in the middle of the coils inside the stator slots in order to identify the highest winding temperature and two in the inlet and outlet oil lines respectively. An oil flow rate of 13.4 litres/min was used. Thermal and flow measurements allowed the calculation of the oil temperature rise (ΔT) and the heat removed by the oil, over 95% in all operating points considered. Machine losses, oil inlet temperature and oil flow rate were used as boundary conditions for the thermal models developed. A comparison between the maximum winding temperatures rise recorded experimentally and those obtained by modelling are shown in Figure 24.

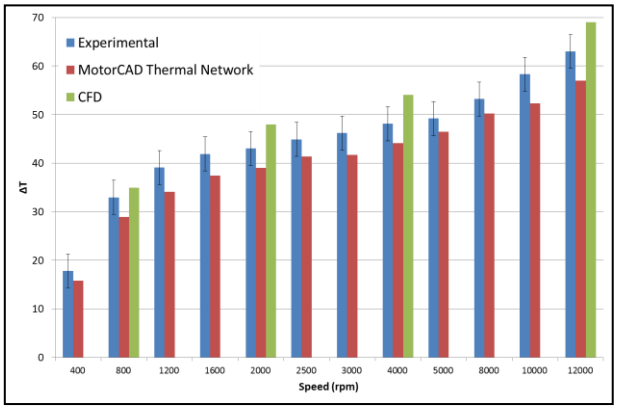

Figure 24 Maximum Windings Temperature rise in the centre of the stator; predicted and measured during a short circuit test

VIII. CONCLUSIONS

This paper has summarized the development of an aircraft starter/generator system which was undertaken as part of the EU CleanSky JTI within The University of Nottingham. The developed S/G is based on active rectification and introduces the fully controlled power electronics into the main path of energy flow. The developed S/G system achieved 16kW/kg for the electrical machine and 4kW/kg for the power electronic converters. The power density is much higher compared with the conventional three-stage S/G solution. In motoring mode, the developed system has demonstrated ability to accelerate the engine to the required speed for ignition with engine friction torque profile under cold-start and hot-start conditions. In generation mode, the S/G system is able to generate the required power under a wide range of speeds and implements droop dc-bus characteristics. This will allow power sharing between different sources in future aircraft DC electric power networks. Flux weakening control is used to allow the electric machine to supply power to the converter at high speed hence reducing the converter rating to cover both operational modes. These S/G systems will be used for further studies including advanced drive control and intelligent DC EPS architecture for MEA applications. Handling conditions is one of the key challenges for the PSMS based S/Gs. Improving the reliability is one direction. In the AEGART project, the Litz wire is used for machine manufacturing for the machine coils. Another mechanism, i.e. auto-declutch rotor from the machine, is the other direction and currently being investigated within the University of Nottingham.

ACKNOWLEDGMENT

The authors gratefully acknowledge the EU FP7 funding via the Clean Sky JTI – Systems for green Operations ITD. The continuity of the AEGART work is currently supported by the Clean Sky 2 Joint Undertaking under the European Union's Horizon 2020 research and innovation program under grant agreement No 807081.

REFERENCES

[1] B. K. Bose, "Global Energy Scenario and Impact of Power Electronics in 21st Century," IEEE Transactions on Industrial Electronics, vol. 60, pp. 2638-2651, 2013.

[2] I. Moir, Aircraft systems: Mechanical, electrical, and avionics subsystems 2008.

[3] Available: http://www.2020-horizon.com/AEGART-AIRCRAFT-ELECTRICAL-GENERATION-SYSTEM-WITH-ACTIVE-RECTIFICATION-AND-HEALTH-MONITORING(AEGART)-s2694.html

[4] J. B. Bartolo, M. Degano, J. Espina, and C. Gerada, "Design and Initial Testing of a High Speed 45 kW Switched Reluctance Drive for Aerospace Application," IEEE Transactions on Industrial Electronics, vol. PP, pp. 1-1, 2016.

[5] D. Gerada, D. Borg-Bartolo, A. Mebarki, C. Micallef, N. L. Brown, and C. Gerada, "Electrical machines for high speed applications with a wide constant-power region requirement," in Electrical Machines and Systems (ICEMS), 2011 International Conference on, 2011, pp. 1-6.

[6] P. Arumugam, Z. Xu, A. L. Rocca, G. Vakil, M. Dickinson, E. Amankwah, et al., "High-Speed Solid Rotor Permanent Magnet Machines: Concept and Design," IEEE Transactions on Transportation Electrification, vol. 2, pp. 391-400, 2016.

[7] P. Arumugam, Z. Xu, G. Vakil, T. Hamiti, S. Bozhko, C. Gerada, et al., "Solid rotor interior permanent magnet machines for high speed applications," in Industrial Electronics Society, IECON 2015 - 41st Annual Conference of the IEEE, 2015, pp. 001741-001746.

[8] Z. Xu, A. L. Rocca, S. J. Pickering, C. Eastwick, C. Gerada, and S. Bozhko, "Mechanical and thermal design of an aeroengine starter/generator," in 2015 IEEE International Electric Machines & Drives Conference (IEMDC), 2015, pp. 1607-1613.

[9] J. Bryan, "Service Factor: What is it and what does it do?," Electrical Apparatus Service Assoication, 2015.

[10] A. La Rocca, "Thermal analysis of a high speed electrical machine," PhD, University of Nottingham, 2016.

[11] M. Degano, P. Arumugam, W. Fernando, T. Yang, H. Zhang, J. B. Bartolo, et al., "An optimized bi-directional, wide speed range electric starter-generator for aerospace application," in Power Electronics, Machines and Drives (PEMD 2014), 7th IET International Conference on, 2014, pp. 1-6.

[12] N. Celanovic and D. Borojevic, "A comprehensive study of neutral-point voltage balancing problem in three-level neutral-point-clamped voltage source PWM inverters," in Applied Power Electronics Conference and Exposition, 1999. APEC '99. Fourteenth Annual, 1999, pp. 535-541 vol.1.

[13] R. Maheshwari, S. Munk-Nielsen, and S. Busquets-Monge, "EMI performance comparison of two-level

and three-level inverters in small dc-link capacitors based motor drives," in Industrial Electronics (ISIE), 2012 IEEE International Symposium on, 2012, pp. 652-657.

[14] S. Bozhko, S. S. Yeoh, F. Gao, and C. Hill, "Aircraft starter-generator system based on permanent-magnet machine fed by active front-end rectifier," in IECON 2014 - 40th Annual Conference of the IEEE Industrial Electronics Society, 2014, pp. 2958-2964.

[15] S. S. Yeoh, F. Gao, S. Bozhko, and G. Asher, "Control design for PMM-based starter generator system for More Electric Aircraft," in Power Electronics and Applications (EPE'14-ECCE Europe), 2014 16th European Conference on, 2014, pp. 1-10.

[16] F. Gao, S. Bozhko, Y. S. Shen, and G. Asher, "Control design for PMM starter-generator operated in flux-weakening mode," in Power Engineering Conference (UPEC), 2013 48th International Universities', 2013, pp. 1-6.

[17] Y. S. Bozhko S, Gao F, Yang T, Hill C. , "Control design for electric starter-generator based on a high-speed permanent-magnet machine fed by an active front-end rectifier," SAE International Journal of Aerospace, 2014.

[18] R. Pena, J. C. Clare, and G. M. Asher, "Doubly fed induction generator using back-to-back PWM converters and its application to variable-speed wind-energy generation," IEE Proceedings - Electric Power Applications, vol. 143, pp. 231-241, 1996.

[19] H. Streifinger, "Fuel/Oil System Thermal Management in Aircraft Turbine Engines," Design principles and methods for aircraft gas turbine engines, 1999.